Proceedings of ASME Turbo Expo 2011
GT2011
June 6-10, 2011, Vancouver, British Columbia, Canada

GT2011-46014

Effects of Pin-Fin Height on Flow and Heat Transfer in a Rectangular Duct

X. Chi[1], T.I-P. Shih[1,2], K.M. Bryden[2], S. Siw[3], M.K. Chyu[3], R. Ames[4], and R.A. Dennis[4]

[1]School of Aeronautics and Astronautics, Purdue University, West Lafayette, IN 47905
[2]Ames Laboratory, U.S. Department of Energy, Ames, IA 50011
[3]Department of Mechanical Engineering and Material Science, University of Pittsburgh, Pittsburgh, PA 15261
[4]National Energy Technology Laboratory, U.S. Department of Energy, Morgantown, WV 26507

ABSTRACT

CFD simulations were performed to study the flow and heat transfer in a rectangular duct (W_d x H_d, where W_d/H_d = 3) with a staggered array of circular pin fins ($D=H_d/4$) mounted on the two opposite walls separated by H_d. For this array of pin fins, five different pin-fin height (H) combinations were examined, and they are (1) $H=H_d=4D$ (i.e., all pin fins extended from wall to wall), (2) H=3D on both walls, (3) H=2D on both walls, (4) H=4D on one wall and H=2D on the opposite wall, and (5) H=3D on one wall and H=2D on the opposite wall. The H values studied give H/D values of 2, 3, and 4 and C/D values of 2, 1, and 0, where C is the distance between the pin-fin tip and the opposite wall. For all cases, the duct wall and pin-fin surface temperatures were maintained at T_w = 313.15 K; the temperature and the speed of the air at the duct inlet were uniform at T_{inlet} = 343.15 K and U = 8.24 m/s; the pressure at the duct exit was fixed at P_b = 1 atm; and the Reynolds number based on the duct hydraulic diameter and duct inlet conditions was Re = 15,000. This CFD study is based on 3-D steady RANS, where the ensemble averaged continuity, compressible Navier-Stokes, and energy equations are closed by the thermally perfect equation of state and the two-equation realizable k-ε turbulence model with wall functions and with the low-Reynolds number model of Chen and Patel in the near-wall region. The usefulness of this CFD study was assessed by comparing predicted heat-transfer coefficient and friction factor with available experimental data. Results are presented to show how the flow induced by arrays of pin fins of different heights affects temperature distribution, surface heat transfer, and pressure loss.

NOMENCLATURE

C	clearance height (distance from the pin-fin tip to the opposite wall)
D	diameter of the pin fin
D_h	duct hydraulic diameter
f	friction factor, $(2D_h/\rho U^2)(dP/dx)$
h	heat transfer coefficient $q''/(T_b - T_w)$
H	height of the pin fin
H_d	height of the duct
k	thermal conductivity
L	length of the test section with the pin fins
L_w	distance between walls to centers of pin fins next to the walls
L_x	distance between pin fins in the streamwise direction
L_y	distance between pin fins in the spanwise direction
Nu	Nusselt number, hD_h/k
P	pressure
Pr	Prandtl number
q”	heat flux (W/m^2)
Re	Reynolds number, $\rho U D_h/\mu$
T	temperature
T_b	bulk temperature
T_w	wall temperature
U	mean velocity in the duct at the inlet
U_τ	friction velocity, $(\tau/\rho)^{0.5}$
W_d	width of the duct
X	coordinate in the streamwise direction
y	normal distance from wall
y^+	$\rho U_\tau y/\mu$
Y	coordinate in the spanwise direction
Z	coordinate in the vertical direction

Greek Symbols

ρ	density
τ	wall shear stress
μ	dynamic viscosity

INTRODUCTION

Advanced gas turbines are designed to operate at increasingly higher turbine inlet temperatures for increased thermal efficiency. Since the inlet temperatures employed are much higher than allowable material temperatures, cooling is needed for all parts of the turbine that come in contact with the hot gases. However, because cooling requires work input, cooling must be achieved effectively with minimum cooling flow and minimum pressure drop. For internal cooling, a variety of heat-transfer enhancement techniques have been used, and these include ribs, pin fins, pedestals (pin fins that extend from one wall to the opposite wall), concavities, and jet impingement.

Previous studies on heat-transfer enhancement by pin fins and pedestals have focused on array configurations and the cross-sectional shapes of the pin fins and pedestals [1-12]. Armstrong & Winstanley [1] provided a review of the literatures up to 1987 on pin fins and pedestals. Van Fossen [2], Al Dabagh & Andrews [3] and Chyu, et al. [4-7] reported heat transfer and pressure characteristics of pin fins and pedestal arrays with different geometries and flow conditions. For pedestals with height nearly equal to its diameter, Chyu, et al. [4] suggested that the magnitude of the area-averaged heat transfer from pin fins and the neighboring endwall is comparable. Won, et al. [8] investigated the heat transfer and the flow structures in a rectangular channel with pin fins. They suggested that the horseshoe vortex wrapping around a pin fin at the endwall and the stagnation flow and wake about each pin fin are major factors for the enhancement in heat transfer. Using a hybrid measurement technique, Chyu, et al. [5] investigated the effects of pin height-to-diameter ratio on the heat transfer from both pin-fin surfaces and endwalls and reported that the increase in pin-fin height leads to a higher overall heat transfer, but with a greater pressure loss. Park et al. [9] performed similar experiments using the naphthalene-sublimation technique to examine the rotation effects on heat transfer at the endwall. The overall averaged results show similar patterns to those from Chyu et al. [5], but rotation was found to induce noticeable differences in heat transfer between the two endwalls.

While pin fins are often used to cool the airfoil's trailing edge, they serve another purpose there, and it is to provide mechanical support in that very thin region with cooling passages in it for cooling. As a result, all pin fins extend from wall to wall in this region and hence the name, pedestal, is used for such a pin fin. For other parts of the airfoil, where the structure of the cooling passage itself is sufficiently robust, the pin fins need not to extend from one wall to the opposite wall for strength. Also, recent developments of the so-called "double-wall," "micro-circuit," or "skin" cooling for the main-body could utilize pin-fins installed in a channel directly beneath the airfoil surface [13-14]. These approaches, when used in conjunction with cooling ducts in the main body section of an airfoil, provide considerable flexibility for design innovation to further improve the level of heat-transfer enhancement.

In this study, the focus is on pin fins that do not extend from one wall to the opposite wall. When there is a gap between the pin fin and the opposite wall, the gap creates an additional source of turbulence generation that could enhance mixing and surface heat transfer. Also, with a gap, the pressure loss is expected to be less since the blockage is less. Relatively few investigators have studied the effects of the gap or clearance between the pin-fin tip and the opposite wall. Virtually all previous studies pertaining to pin-fin-tip clearance effects were directed at studying the heat transfer over the portion of the cooling duct wall that were not covered by pin fins. The experimental study by Steuber & Metzger [15], who used short wooden pins that are attached directly to a heated wall and do not touch the opposite wall, is probably one of the earliest studies of this kind. Their study used pins made of wood so that pins are heat-transfer inactive. Also, in their study, the diameter of the pins was made equal to the height of the channel so that the pin-fin height-to-diameter ratio is always less than unity. Their results suggested that pin-fin arrays with shorter length pins consistently lead to lower heat-transfer rates and reduced pressure loss. Arora & Abdel-Messeh [16] later performed a similar study using a wide aspect ratio channel. They concluded that the average heat transfer rate decreases linearly with an increasing value of clearance height to pin diameter (C/D) ratio. Chang, et al. [10] measured the heat transfer from the endwall with C/D ranging from 0 to 0.75. In their study, with pins made of Teflon and so are also heat-transfer inactive, they found an increase in the tip clearance changes the nature of horseshoe vortices as well as the wakes and the separated shear layer downstream to a pin, which collectively reduces the endwall heat transfer and overall pressure loss. However, if the performance index is "heat-transfer enhancement per unit pressure drop", then C/D = 0.25 emerges as the optimal instead of pin fins that extend from wall to wall. Similar studies on the tip-clearance effects for square pins (prisms) relevant to the cooling of electronic components and wind engineering have also been performed [11,12]. Unlike the aforementioned studies on circular pin fins, the square pins are heated, whereas the endwall is kept adiabatic. Dogruoz, et al. [12] experimentally investigated the effects of clearance for square prisms with C/D from unity to eight and reported that the value of C/D has little effect on heat transfer provided that the clearance is sufficiently large. On the other hand, pressure drop decreases as C/D increases over the entire range of C/D investigated.

Siw, et al. [17] experimentally studied a staggered array of pin fins with different pin-fin heights that resulted C/D = 0, 1, and 2 in which the pin fins are also involved in the heat transfer. They used transient liquid crystal technique [18-21] to measure the surface heat transfer coefficient. In that study, they found an increase in C/D to lower heat-transfer enhancement and pressure drop with C/D = 1 exhibiting the highest heat-transfer enhancement, followed by C/D = 0 and C/D = 2.

The objective of this study is to computationally study the experimental study of Siw, et al. [17] with the goal of providing additional insights on how pin fins' C/Ds and H/Ds affect the flow, pressure drop, and surface heat transfer. The organization of the remainder of this paper is as follows. First, the problem studied is described. Then, the problem formulation, the numerical method of solution, and the results generated are presented and discussed.

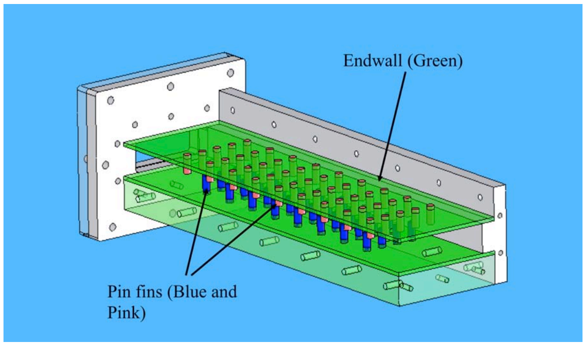

Fig. 1. Schematic of the experimental test section.

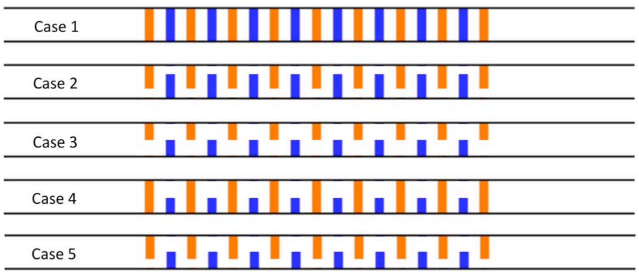

Fig. 2. Schematic of the cases studied (Table 1).

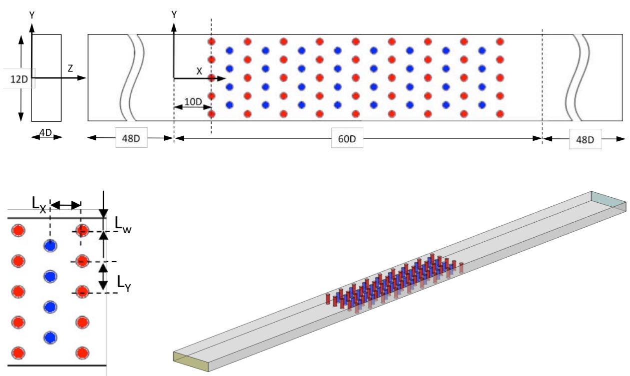

Fig. 3. Schematic of the computational domain.

Table 1: Summary of Cases

Case No.	C/D	H/D: top wall	H/D: bottom wall
1	0	4	4
2	1	3	3
3	2	2	2
4	0 and 2	4	2
5	1 and 2	3	2

DESCRIPTION OF THE PROBLEM

In this section, the problem studied is described. Figure 1 shows the experimental test section of Siw, et al. [17]. This test section is a rectangular duct with width (W_d) of 76.2 mm (3 inches or 12D, D=0.25 inches) and height (H_d) of 25.4mm (1 inch or 4D). Within this duct, a staggered array of pin fins is mounted. Each pin fin has diameter (D) of 6.35 mm (1/4 inch). The pin fins are arranged in a staggered fashion with the spacing in the streamwise direction (L_x) and the spacing in the spanwise direction (L_y) being 2.5D (measured from the center of the pin fins). The distance of the pin fins closest to the walls (L_w) are D from the wall (again measured from the center of the pin).

A number of pin fin heights were investigated, and they are C/D = 0, 1, and 2 and H/D = 4, 3, 2. All cases studied are summarized in Table 1 and illustrated in Fig. 2. In Fig. 2, the red colored pin fins are mounted on the top wall, while the blue colored pin fins are mounted on the bottom (opposite) wall. There are a total of 17 rows of pin fins with nine rows of pin fins with five pins per row mounted on the top wall and eight rows of pin fins with four pin fins per row mounted on the bottom wall. On the top wall, there are a total of 45 pin fins. On the bottom wall, there are a total of 32 pin fins.

In the experiment, the channels walls are made of plexiglas. The low thermal conductivity of plexiglas is necessary for the one-dimensional, semi-infinite heat transfer model on which the local heat transfer coefficient on the surface in between the adjacent pins is based. For the pin fins, they are made of aluminum to ensure very small Biot number so that each pin can be considered as a lump unit with uniform temperature when computing heat transfer coefficient on the pin-fin surfaces. The transient liquid crystal technique [18,19] is used in this study to measure the surface heat transfer coefficient. The detailed operating principle of the hybrid measurement technique is given in Chen and Chyu [20,21] with uncertainty analysis based on Kline and McClintock [22].

. The computational model of the experimental study is shown in Fig. 3. The geometry of the computational model is identical to that of the experimental model in the test section. They differ, however, in the duct upstream and downstream of the test section. The assortment of ducts upstream of the test section in the experiment was replaced by a straight duct of the same cross section as the cross section of the duct at the test section in the computational study. Thus, some effects of the turbulence and secondary flows upstream of the test section in the experiment will not be accounted for. Also, a duct with the same cross section as that of the test section was appended to the test section to ensure that flow conditions at the outflow boundary is nearly uniform with no flow reversal, and this is important for the accuracy of the CFD solutions.

On operating conditions, for all cases in Table 1, the duct wall and pin-fin surface temperatures were maintained at T_w = 313.15 K; the temperature and the speed of the air at the duct inlet were uniform at T_{inlet} = 343.15 K and U = 8.24 m/s; the pressure at the duct exit was P_b = 1 atm. Siw, et al. [17] generated data for several Reynolds numbers. In this computational study, the Reynolds number simulated was Re = 15,000 based on the hydraulic diameter of the unobstructed duct cross-section (D_h) and the bulk mean momentum (ρU) with dynamic viscosity evaluated at the duct inlet temperature.

FORMULATION OF PROBLEM, NUMERICAL METHOD OF SOLUTION, AND CODE

In this study, the governing equations used are the ensemble-averaged continuity, compressible Navier-Stokes, and energy equations for an ideal gas. The effects of turbulence were modeled by the two-equation realizable k-ε model [23] with and without wall functions. For the cases without wall functions, integration of all equations is to the wall, resolving the low-Reynolds number region of the turbulent boundary layers. In the near-wall region, the two-layer model of Chen and Patel [24] is used. This model divides the turbulent flow field into two regions. One region, referred to as the wall region, extends from the wall to the edge of the fully turbulent region. The other region, referred to as the core region, contains the rest of the turbulent flow field which is fully turbulent everywhere. In the wall region, the one-equation model of Wolfshtein [25] is used for the turbulent kinetic energy and an algebraic model is used for the length scale. In the core region, the realizable k-ε model is used.

Solutions to the governing equations were obtained by using the ANSYS Fluent Version 12.0 code [26]. Since only steady-state solutions were sought, the pressure-based segregate solver is selected to generate solutions. In particular, the SIMPLE pressure-velocity coupling scheme is used. All equations were integrated over each cell of the grid system or mesh. The fluxes for all equations at the cell faces were interpolated by using the second-order upwind scheme. Pressure equation was computed by using second-order accuracy.

For all computations, iterations were continued until all residuals for all equations plateau to ensure convergence to steady state has been reached. At convergence, the scaled residuals were always less than 10^{-5} for the three components of the velocity, less than 10^{-7} for the energy, less than 10^{-5} for turbulent kinetic energy, less than 10^{-4} for dissipation rate of turbulent kinetic energy, and less than 10^{-3} for the continuity equation.

The mesh for the computational domain was generated by using Gambit code with map and cooper scheme plus boundary-layer control. To generate the mesh, the computation domain was divided to 3 zones: leading zone, test-section zone, and trailing zone. All cells generated are quadrilateral. Two set of grids were used. One, referred to as the baseline grid, has 3.5 millions cells in total. In the test-section, it has 41 grid points along the duct height (Z-direction, Fig. 3), about 101 grid points along the spanwise direction (Y), and about 800 grid points along the streamwise direction (X). The cells in the leading and trailing zones are stretched so there are only 101 grid points along the streamwise direction for each of those zones. Each pin fin's circumferential direction is resolved by 49 grid points. The grid spacing of the first cell normal to the top wall is 6.35 x 10^{-4} m, which produces y^+ values between 10 and 20. This grid is used with Fluent's "enhanced wall treatment" wall function option, which allows the y^+ value to be lower than typical 30 or 40 that are needed to enter the log-law layer. A smaller y^+ value was used in order to capture some of the physics of the horseshoe vortex at the base of each pin fin. Figure 4 shows the baseline mesh for Case 1 (Table 1).

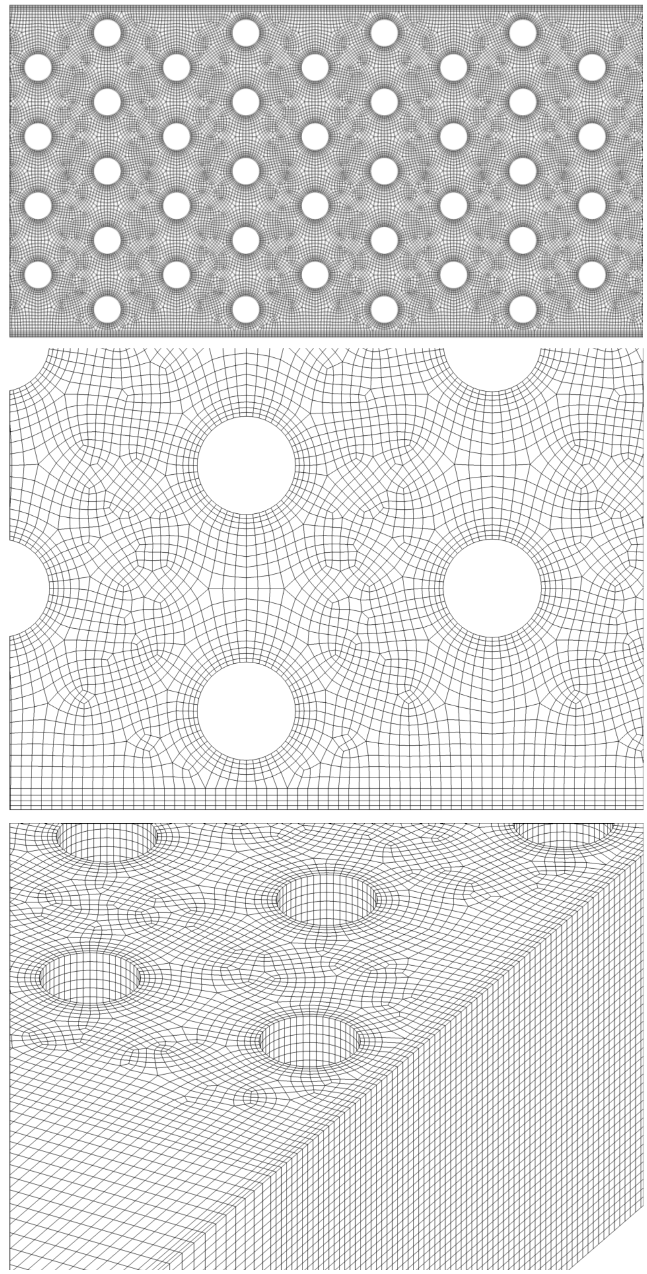

Fig. 4. Baseline mesh used for Case 1 (Table 1).

The second mesh, referred to as the fine mesh, is intended to be run with the low Reynolds number turbulence model, where the integration of all equations is to the wall so that the y^+ values of all first cells away from walls is less than unity. For the C1 configuration, this fine mesh has 11.5 million cells for just one quarter of the computation domain. The symmetry of the C1 configuration with pin fins extending from top wall to bottom wall allows for this partitioning. For the fine mesh, 51 grid points are distributed along the duct height (half of channel height), about 91 grid points are distributed along the spanwise direction (half the channel width), and about 800 grid points are distributed along the streamwise direction. About 101 points are distributed along each pin fin's circumference direction. The grid spacing of the first cell normal to the top wall is 1.27 x 10^{-5} m. For the finer mesh, not only is the y^+ less than unity next to all solid surface (walls of the duct and pin-fin surfaces), the resolution in the interior of the flow domain is also almost doubled. Figure 5 shows the fine mesh generated for the C1 configuration.

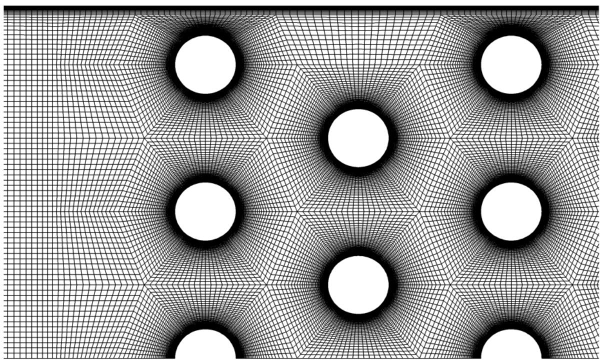

Fig. 5. Grid about a pin fin in the fine mesh for Case 1.

RESULTS

This section on results is organized into three parts. The first part addresses the issue of wall functions (baseline mesh) versus low-Reynolds number turbulence model (fine mesh) in predicting the flow and heat transfer for the Case 1 (Table 1) configuration. The second step compares predicted results with experimental measurements for Case 1. Thus, the first two parts are aimed at grid sensitivity and validation. Once the error bounds in the computational analysis are assessed, the third part presents the results generated for the five cases in Table 1.

Wall Function versus Low-Re Number Model

Figures 6 to 9 compare results generated by using wall functions (WF) on the baseline mesh (Fig. 4) with the results generated by using a low-Reynolds number turbulence model (low-Re) on a fine mesh (Fig. 5). From Figs. 6 and 7, it can be seen that the temperature and velocity magnitude distribution in the middle plane (Z=0) predicted by WF and by low-Re are nearly the same. This indicates that the stagnation and wake flow about each pin fin away from the walls are captured by both the baseline and the fine meshes. Figures 8 and 9 compare the predictions about the wall, where the boundary layer next to the wall forms a horseshoe vortex about each pin fin. Figures 8 and 9 show the predicted surface heat transfer to be qualitative similar, but quantitatively quite different, at least locally. Basically, low-Re on the fine mesh predicted much higher heat transfer on the wall upstream of each pin fin when compared to WF on the baseline mesh. This is expected since the horseshoe vortex about each pin fin at the base of pin fin is better resolved by the low-Re on the fine mesh. Though there are considerable differences in heat transfer locally, the difference in the total heat transferred to the top and bottom walls is not high. It is 65.36 W for the low-Re and 61.90 W for the WF, which gives a percent difference of 5.4%. This indicates WF to give reasonable results on overall heat transfer rate when compared to low-Re. This is important since the low-Re model requires much more cells than WF (11.5 x 4 million versus 3.5 million for a complete duct).

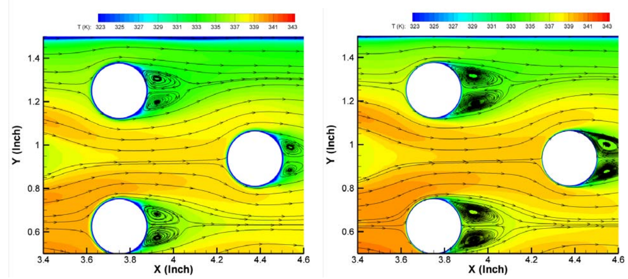

Fig. 6. Temperature and streamlines in middle plane (Z=0) for Case 1. Left: WF on baseline mesh. Right: low-Re on fine mesh.

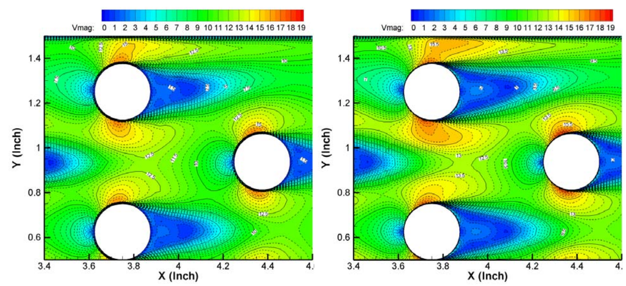

Fig. 7. Velocity magnitude (Vmag, m/s) in middle plane (Z=0) for Case 1. Left: WF on baseline mesh. Right: low-Re on fine mesh.

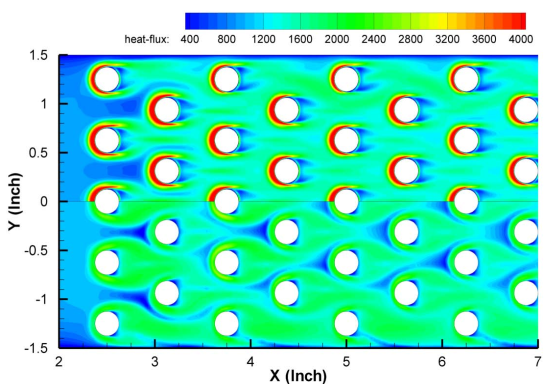

Fig. 8. Heat flux (q", W/m^2) on top/bottom wall. Top half: Case 1 with fine mesh. Bottom half: Case 1 with baseline mesh.

Comparing CFD Predictions with Experimental Data

Figure 10 shows the computed and measured heat-transfer coefficient ($h = q"/(T_w - T_b)$) on the top/bottom wall for Case 1 in Table 1. Throughout this study, the bulk temperature (T_b) needed to compute h is given by linearly interpolating T_b computed at the beginning of the "test section" and the T_b computed at the end of the "test section" of the computational domain.

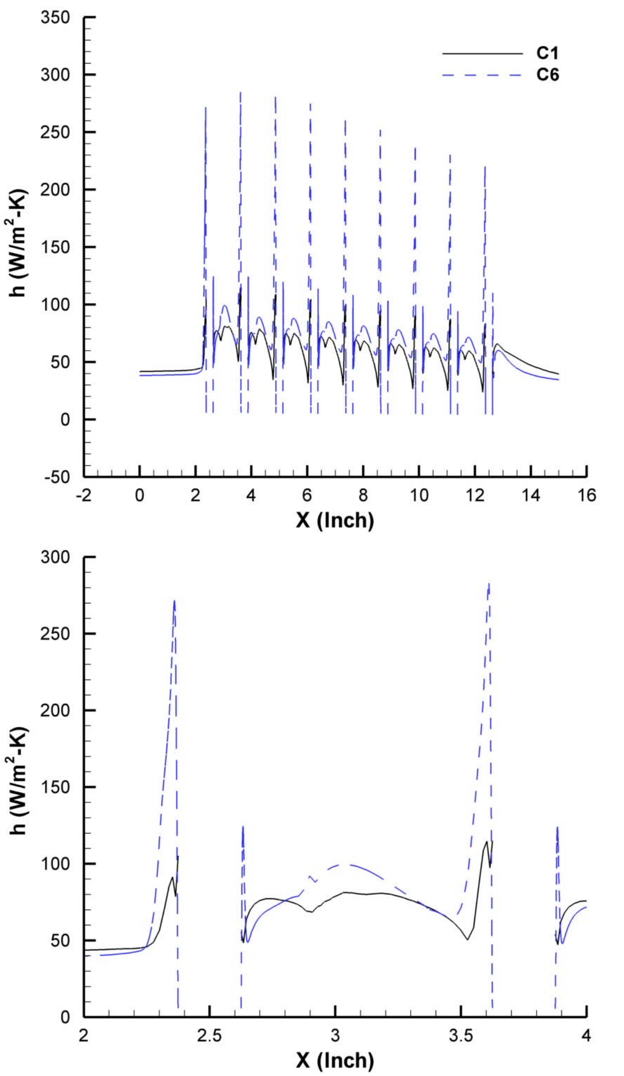

Fig. 9. Heat-transfer coefficient along center line (Y=0) on top/bottom wall for Case 1. C1 denotes baseline mesh and C6 denotes fine mesh.

From Fig. 10, it can be seen that the resolution of the experiment and the resolution of the CFD are different. The resolution of the experiment is such that it averages some peaks and valleys in the data. However, the overall features can still be seen such as the high heat transfer on the duct wall just upstream of each pin and the increased heat transfer downstream of each pin fin from the horseshoe vortex that wraps around each pin fin. Qualitatively, the distribution of the heat-transfer coefficient predicted by CFD appears to agree with the experimental measurement. Quantitatively, however, CFD predictions were lower than the measured data by as much as 30 to 40%. This indicates that both the enhanced wall function and the two-layer model used are unable to capture the heat transfer in the near-wall region with sufficient accuracy quantitatively.

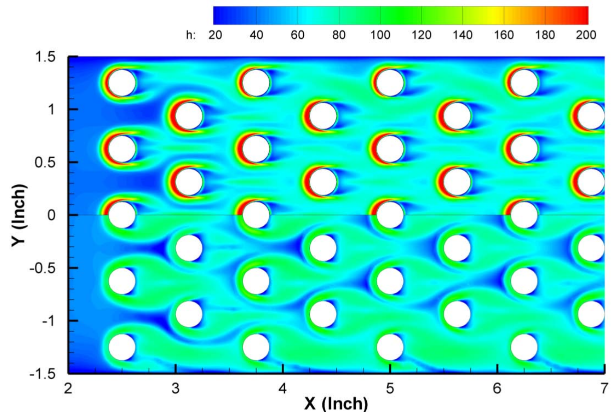

(a) CFD prediction (this study). Top Half: low-Re model on fine mesh. Bottom Half: WF on baseline mesh.

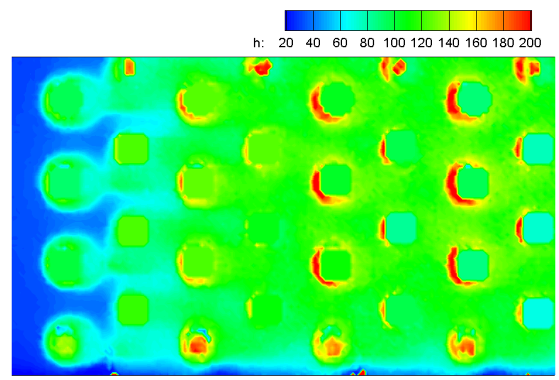

(b) Experimental measurement (Siw, et al. [17]).

Fig. 10. Measured heat-transfer coefficient (h, W/m^2-K) on top/bottom wall for Case 1.

Figure 11 shows the computed and the measured normalized friction factor f/f_0 for all five cases in Table 1. The f in f/f_0 is defined by $(2D_h/\rho U^2)(dP/dx)$. As can be seen in Fig. 12, the pressure gradient in the region containing the pin fins vary almost linearly. Thus, dP/dx is approximated by (average pressure at X = 317.5 mm (S17) – average pressure at X = 63.5 mm (S1)) / (317.5 mm – 63.5 mm); see Fig. 12 on the location of S1 and S17 The f_0 in f/f_0 is the friction factor for a fully developed turbulent flow in a smooth channel. The formula developed by Petukhov was used in this study, and it is

$$f_o = (0.790 \ln Re - 1.64)^{-2} \quad 3000 \le Re \le 5x10^6$$

In Fig. 11, the CFD results were obtained by using the "enhanced wall function" on the baseline grid with and without pin fins to get f and f_o. Figure 11 shows the CFD with enhanced wall functions can capture the friction factor with reasonable accuracy.

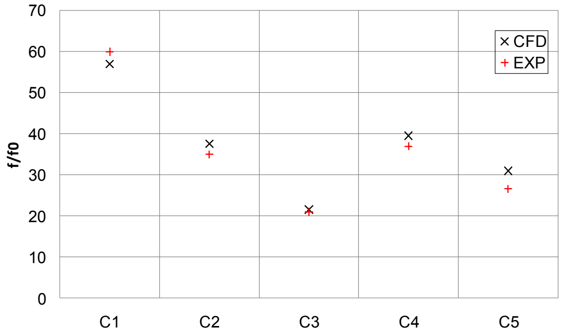

Fig. 11. Normalized friction factor, where C# denotes Case # in Table 1.

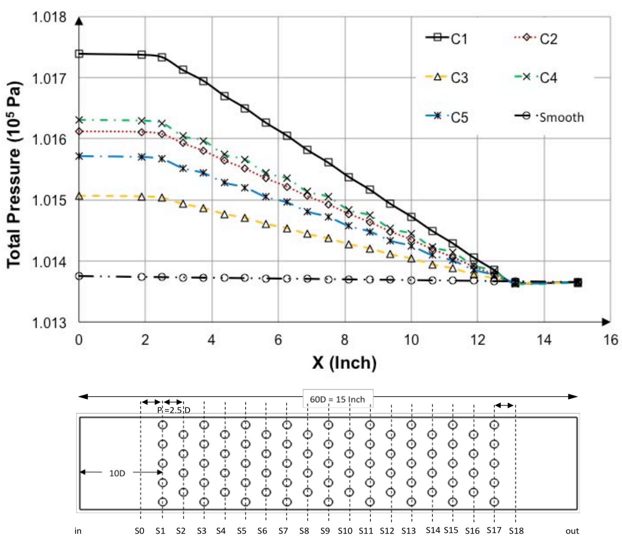

Fig. 12. Variation of average stagnation pressure along duct (symbols denotes locations where pressure was averaged). C# denotes Case # in Table 1.

Effects of Pin-Fin Height on Flow and Heat Transfer

Figure 12 shows the variation of the stagnation pressure along the test section for all five cases. From this figure, it can be seen that pressure loss is a strong function of C/D. The lower the C/D, the higher the pressure loss.

Figures 13 to 18 show the CFD results obtained on the baseline mesh with the enhanced wall functions invoked for the five cases in Table 1. Figure 13 show the temperature distribution in the middle plane between the top and bottom walls with projected streamlines. From this figure, a wake can be seen behind each pin fin that extend beyond the middle plane. Though not shown in detail, the wake behind each pin fin consists of a pair of counter-rotating vortices that do not shed. The size of this wake is largest at the base of the pin fin where the wake and the horseshoe vortex interact. This figure also shows the thermal boundary layer from the two side walls and about each fin.

Figure 14 shows the shear stress on the top and bottom walls, where the pin fins are mounted. Shear stress on the top and bottom walls is high when the flow is accelerated around each pin fin and when the horseshoe vortex wrapped around each pin fin. It is also higher when there is clearance height between the wall and pin fin mounted on the opposite wall. This is because the tip of each pin fin induces a separated region and creates additional turbulence for mixing. The shear stress is low near stagnation regions and where streamlines come together. Heat transfer rate is expected to be high in the region about the stagnation zone, and regions where streamlines converge because the fluid away from wall is transported to the wall, which will increase the temperature gradient. Heat flux is also expected to be high where turbulence is high since it increases mixing.

Figure 15 shows the local heat flux about pin fins at the top and bottom walls where the pin fins are mounted. When the pin fins extended from wall to wall (Case 1: C/D=0 & H/D=4), the heat flux on the top and bottom walls is highest just upstream and around every pin fin because of the horseshoe vortex about each pin fin. The heat flux is lowest in regions just upstream of the horseshoe vortices, where the flow is slowing down and the two separated regions just behind the pin fins. For Case 2 (C/D=1 & H/D=3), where pin fins from opposite walls extend to three-forth of the duct height, heat flux is also high in regions between pin fins in the streamwise direction because of the turbulence and separation created at the tip of the pin fins from the opposite wall. For this case, locations of the minimum heat flux are in the two separated regions just behind each pin fin and where streamline converge but move away from the walls (instead of towards the wall) located at about D upstream of and mid way between the columns of pin fins in the spanwise (Y) direction. For Cases 3 to 5, where pin fins on opposite walls extend to greater or less than the pin fins in Case 2, one can see the effects of the clearance height on heat transfer.

Figure 16 shows the heat transfer coefficient computed on the top wall for all five cases. Figures 17 and 18 show the heat-transfer coefficient along the centerline (Y=0) on the top and bottom walls. These figures show the effects of clearance height in a quantitative way.

Effects of C/D and H/D

Figures 19 to 21 show the net heat transferred. Figure 19 shows that Case 1 (C/D=0, H/D=4) has the highest overall heat transfer, which is followed by Case 2 (C/D=1, H/D=3), Case 4 (C/D=0, H/D=4 & C/D=2, H/D=2), Case 5 (C/D=1, H/D=3 & C/D=2, H/D=2), and Case 3 (C/D=2, H/D=2). The main reason is that heat transfer from the pin fins dominated, and their order from high to low is the same as that given above, and it is based on total surface area of the pin fins.

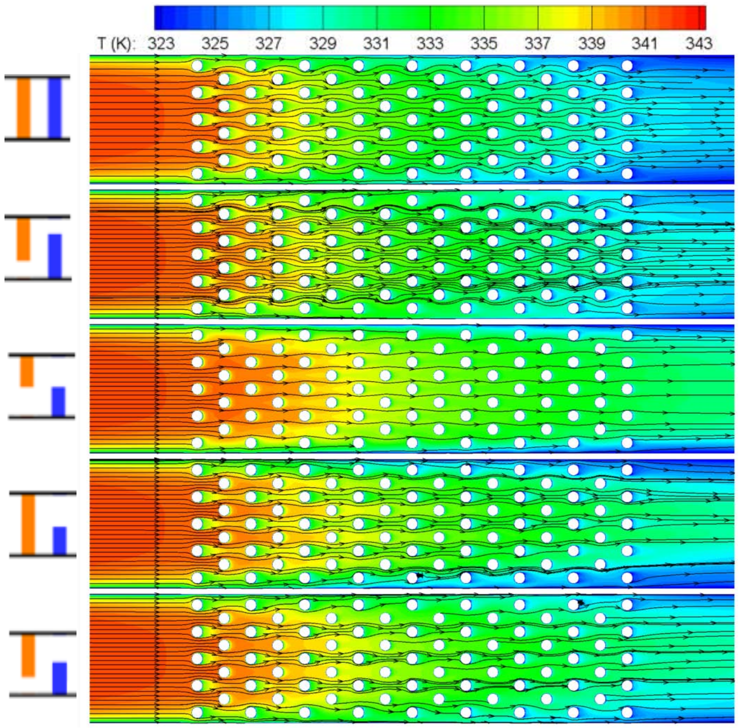

Fig. 13. Temperature with projected streamlines in mid plane (Z=0).

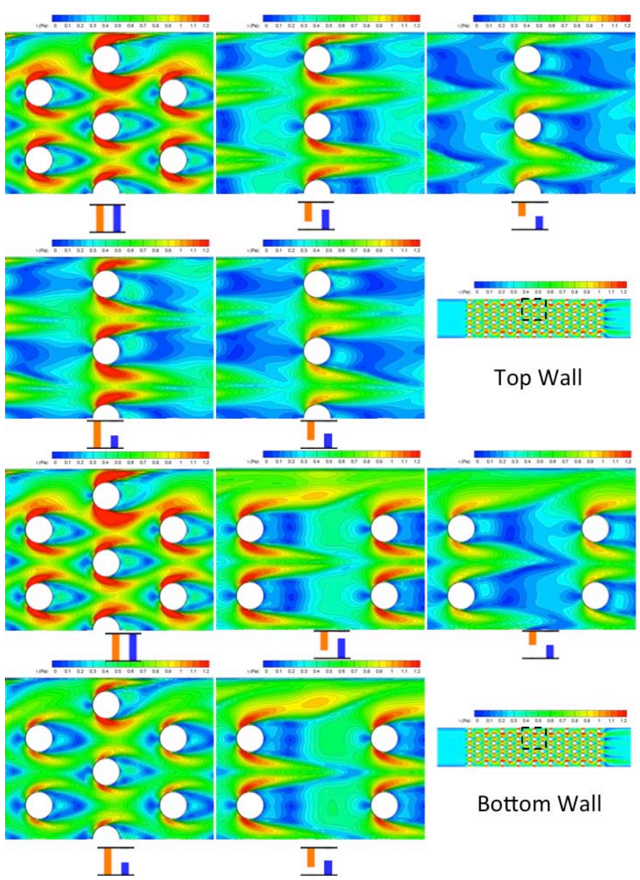

Fig. 14. Shear stress (Pa) on top and bottom walls.

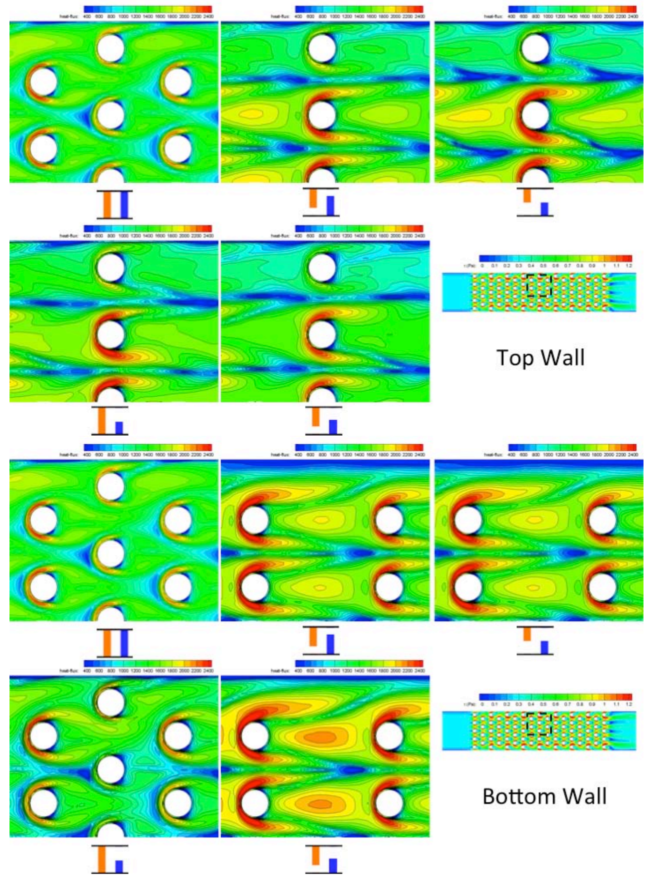

Fig. 15. Heat flux on top and bottom walls.

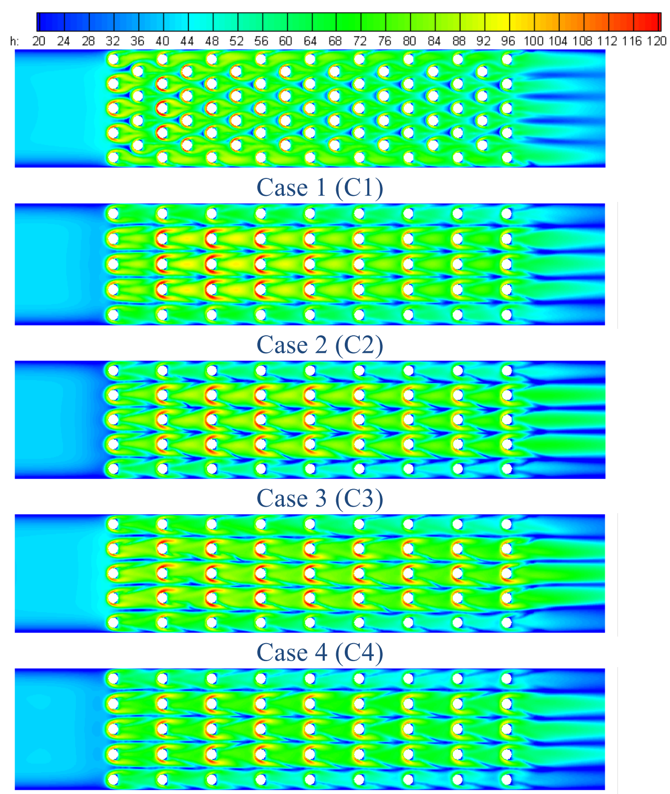

Fig. 16. Computed heat-transfer coefficient on the top wall.

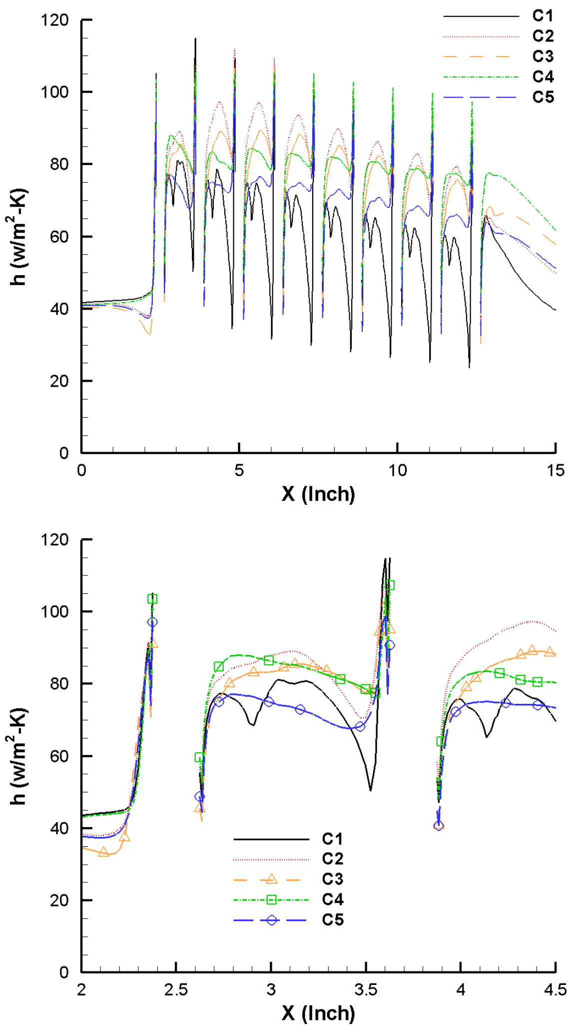

Fig. 17. Computed heat-transfer coefficient along center line of top wall (Y=0, Z=H_d). C# denotes Case # in Table 1.

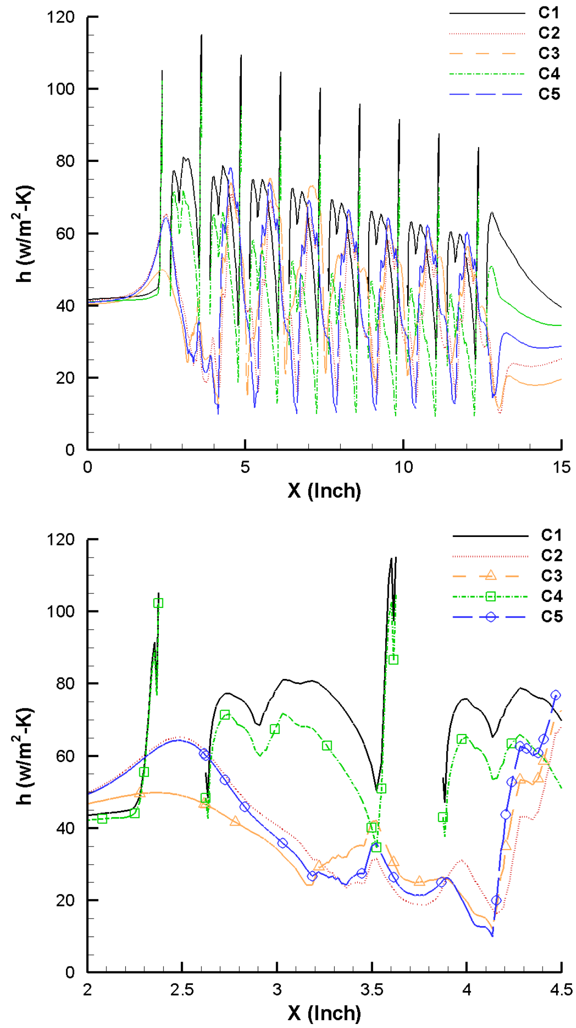

Fig. 18. Computed heat-transfer coefficient along center line of bottom wall (Y=0, Z=0). C# denotes Case # in Table 1.

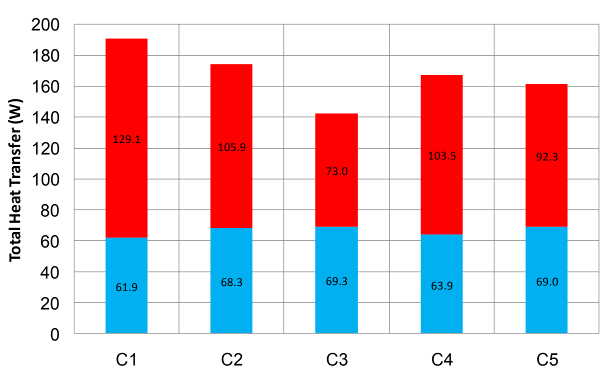

Fig. 19. Heat transfer contribution by pin fins (red) and top and bottom walls

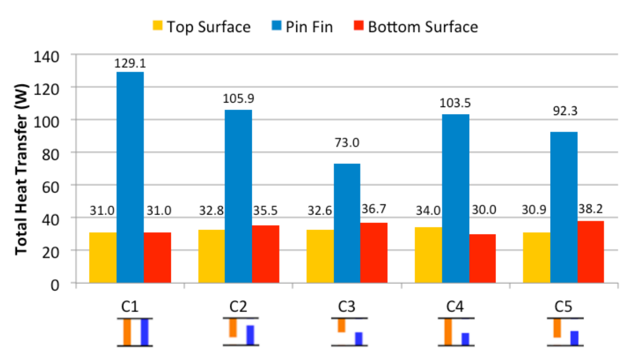

Fig. 20. Total heat transfer from top wall, bottom wall, and pin fins in test section for the five cases studied.

If only the heat transfer from the top and bottom walls are considered, then Case 3 has the highest heat transfer, followed by Case 5, Case 2, Case 4, and Case 1. The percent difference between Case 3 and Case 1 is only 11.1%. Thus, the effects of the C/D and H/D is not high from the heat transfer perspective. Figure 20 gives more details on the heat transfer from the top wall and the heat transferred from the bottom wall. Though there are differences, they are not significant.

Figure 21 gives the heat-transfer enhancement in terms of Nu_T normalized by Nu_0 for a smooth duct. Nu_o is based on the Dittus-Boelter correlation for forced convection turbulent flow inside smooth ducts, and is given by

$$Nu_0 = 0.023 Re^{0.8} Pr^{0.3}$$

The power on the Pr number is 0.3 because the wall is cooler than the fluid. The magnitude of Nu_T is calculated by combining the contribution from both endwalls and pin-fins and weighted by the size of the wetted area; i.e.,

$$Nu_T = \frac{\sum Nu_p \times A_p + \sum Nu_w \times A_w}{\sum A_p + \sum A_w}$$

In terms of Nu_T/Nu_0, Case 1 has the highest heat-transfer enhancement at about 2.75, followed by Case 2 (2.6), Case 4 (2.5), Case 5 (2.5), and Case 3 (2.25).

Figure 22 shows the loss in stagnation pressure for the five cases. The loss in stagnation pressure is the lowest for Case 3 (142.5 Pa), followed by Case 5, Case 2, Case 4, and Case 1 (373.2 Pa). The percent difference from the highest and the lowest at 61.8% is significant. Pressure loss is primarily due to H/D or the surface area of the pin fins' side walls.

Figure 23 shows the total heat transfer in the test section divided by the loss in stagnation pressure across the test section. Though this parameter is dimensional, it gives a measure of two important objectives, namely high heat transfer and low pressure drop. Based on this parameter, Case 3 (C/D=2, H/D=2) is best, followed by Case 5, Case 2, Case 4, and Case 1.

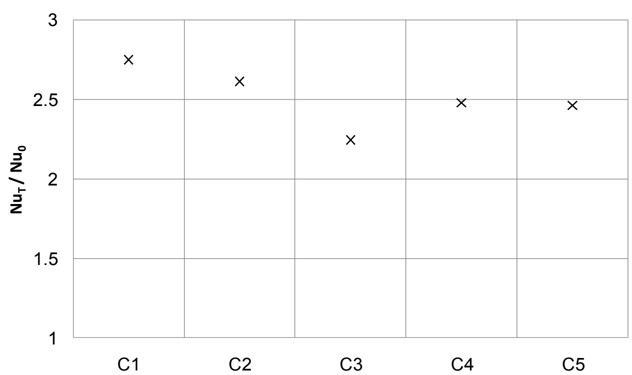

Fig. 21. Heat transfer enhancement, Nu_T/Nu_0, where Nu_0 is for the smooth duct without pin fins.

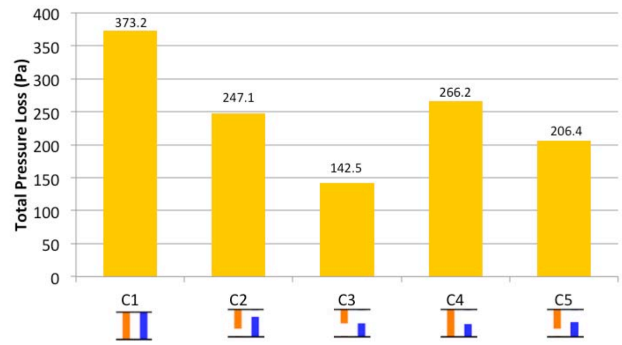

Fig. 22. Total loss in stagnation in test section for the five cases studied.

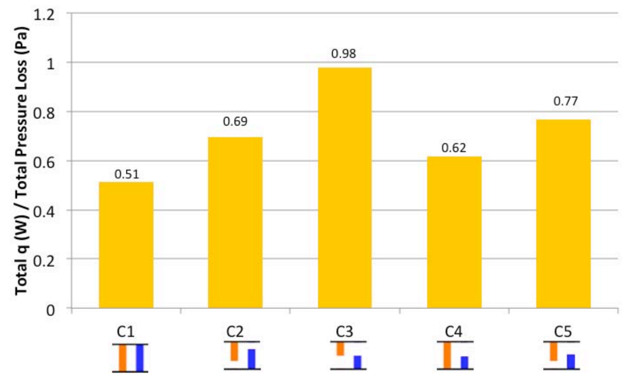

Fig. 23. Performance metric - total heat transfer/total pressure loss - for the five cases studied.

CONCLUSIONS

This CFD study based on steady RANS with the realizable k-ε model and "enhanced" wall functions (y^+ of the first cell between 10 and 20) show that pin fins' clearance height-to-diameter ratio (C/D) and height-to-diameter ratio (H/D) have significant effects on surface heat transfer and loss in stagnation pressure. Of the C/D (0, 1, and 2) and H/D (4, 3, 2) studied at a duct Reynolds number of 15,000, it was found that the heat transferred from the pin fins were higher than the heat transfer from the two walls on which the pin fins are mounted. For the range of parameters studied, the lower the C/D, the higher is the heat transfer and the loss in stagnation pressure. Conversely, the higher the C/D, the lower is the heat-transfer and the loss in stagnation pressure. Based on the parameter, the ratio of total heat-transferred to total loss in stagnation pressure, the case with C/D=2 and H/D=2 was found to be the best.

ACKNOWLEDGMENT

This research was supported by the Department of Energy's National Energy Technology Laboratory. The authors are grateful for this support.

REFERENCES

1. Armstrong, J. and Winstanley, D., 1988, "A Review of Staggered Array Pin Fin Heat Transfer for Turbine Cooling Applications," *ASME J. of Turbomachinery*, Vol. 110, pp. 94-103.
2. Al Dabagh, A. M., and Andrews, G.E., 1992, "Pin-Fin Heat Transfer: Contribution of the Wall and the Pin to the Overall Heat Transfer," ASME Paper 92-GT-242.
3. VanFossen, G.J., 1982, "Heat Transfer Coefficients for Staggered Arrays of Short Pin Fins," *ASME J. Eng. Power*, Vol. 104, pp. 268-274.
4. Chyu, M.K., Hsing, Y.C., Shih, T.I-P., and Natarajan, V., 1999, "Heat Transfer Contributions of Pins and Endwall in Pin-Fin Array: Effects of Thermal Boundary Condition Modeling," *ASME J. of Turbomachinery*, Vol. 121, pp. 257-263.
5. Chyu, M.K., Siw, S. and Moon, H.K., 2009, "Effects of Height-to-Diameter Ratio of Pin Element on Heat Transfer from Staggered Pin-Fin Arrays," GT2009-59814.
6. Chyu, M.K., and Goldstein, R.J., 1991, "Influence of an Array of Wall-Mounted Cylinders on the Mass Transfer from a Flat Surface," *Int. J. of Heat Mass Transfer,* Vol. 34, No. 9, pp. 2175-2186.
7. Chyu, M.K., 1990, "Heat Transfer and Pressure Drop for Short Pin-Fin Arrays and Pin-Endwall Fillet," ASME J. of Heat Transfer, Vol. 112, No. 4, pp. 926-932.
8. Won, S.Y., Mahmood, G.I., and Ligrani, P.M., 2004, "Spatially-Resolved Heat Transfer and Flow Structure in a Rectangular Channel with Pin Fins," *Int. J. of Heat and Mass Transfer*, Vol. 47, pp. 1731-1743.
9. Park, J.S., Kim, K.M., Lee, D.H., Cho, H.H., and Chyu, M.K., 2008, "Heat Transfer on Rotating Channel With Various Height of Pin Fins," ASME Paper GT2008-50783.
10. Chang, S.W., Yang, T.L., Huang C.C., and Chiang, K.F., 2008, "Endwall Heat Transfer and Pressure Drop in Rectangular Channels with Attached and Detached Circular Pin–Fin Array," Int. Journal of Heat and Mass Transfer, 51, pp. 5247-5259.
11. Sara, O.N., 2003, "Performance Analysis of Rectangular Ducts with Staggered Square Pin Fins," Energy Convers. Manage, Vol. 44, pp. 1787-1803.
12. Dogruoz, M.B., Urdaneta, M., and Ortega, A., 2005, "Experiments and Modeling of the Hydraulic Resistance and Heat Transfer of In-line Square Pin fin Heat Sink with Top By-pass Flow," Int. J. of Heat and Mass Transfer, 48, pp. 5058-5071.
13. Lafleur, Ronald S, United Technologies Corporation, Method for Cooling a Wall Within a Gas Turbine Engine, EP 1 617 043 B1. 2008.
14. Chyu, M.K., Siw, S., Karaivanov, V., and Alvin, M.A., 2009, "Aerothermal Challenges in Syngas,Hydrogen-Fired and Oxy-fuel Turbines: Part II – Effects of Internal Heat Transfer," ASME J. of Thermal Science and Engineering Applications, Vol. 1, 011003.
15. Steuber, G.D., and Metzger, D.E., 1986, "Heat Transfer and Pressure Loss Performance for Families of Partial Length Pin Fin Arrays in High Aspect Ratio Rectangular Ducts," 8th International Heat Transfer Conference, Vol 6, pp. 2915-2920.
16. Arora, S.C. and Abdel-Messeh, W., 1989, "Characteristics of Partial Length Circular Pin Fins as Heat Transfer Augmentators for Airfoil Internal Cooling Passages," ASME Paper 89-GT-87.
17. Siw, S.C., Chyu, M.K., Shih, T.I-P., and Alvin, M.A., 2010, "Effects of Pin Detached Space on Heat Transfer in in Fin Arrays," ASME Paper GT2010-23227.
18. Metzger, D.E. and Larson, D.E., 1986, "Use of Melting Point Surface Coatings for Local Convection Heat Transfer Measurements in Rectangular Channel Flows with 90-Deg Turns," *J. of Heat Transfer*, Vol. 109, pp. 48-54.
19. Chyu, M.K. Ding, H., Downs, J.P. and Soechting, F.O., 1998, "Determination of Local Heat Transfer Coefficient Based on Bulk Mean Temperature Using a Transient Liquid Crystal Technique," *J. of Experimental Thermal and Fluid Science*, Vol. 18, pp. 142-149.
20. Chen, S.P., Li, P.W., and Chyu, M.K., 2006, "Heat Transfer in a Airfoil Trailing Edge Configuration with Shaped Pedestals Mounted Internal Cooling Channel and Pressure Side Cutback," ASME Paper GT2006-91019.
21. Chyu, M.K., Oluyede, E.O., and Moon, H-K., 2007, "Heat Transfer on Convective Surfaces with Pin-Fins Mounted in Inclined Angles," GT2007-28138.
22. Kline, S.J. and McClintock, F.A., "Describing Uncertainties in Single Sample Experiments," Eng. (Am. Soc. Mech. Eng.), Vol. 75, pp. 3-8.
23. Shih, T.-H., Liou, W., Shabbir, A., and Zhu, J., "A New k-ε Eddy-Viscosity Model for High Reynolds Number Turbulent Flows – Model Development and Validation," *Computers and Fluids*, Vol. 24, No. 3, 1995, pp. 227-238.
24. Chen, H.C. and Patel, V.C., "Near-Wall Turbulence Models for Complex Flows including Separation," *AIAA Journal*, Vol. 26, No. 6, 1988, pp. 641-648.
25. Wolfshtein, M., "The Velocity and Temperature Distribution in One-Dimensional Flow with Turbulence Augmentation and Pressure Gradient," *International Journal of Heat and Mass Transfer*, Vol. 12, 1969, pp. 301-318.
26. http://www.ansys.com/products/fluid-dynamics/fluent/